

New magnetic states in nanorings created by anisotropy gradients

M. Castro, A.P. Espejo, D. Altbir, and S. Allende

*Departamento de Física, Universidad de Santiago de Chile and CEDENNA,
Avda. Ecuador 3493, Santiago, Chile*

N.M. Vargas

Department of Physics, University of California, San Diego, La Jolla, California 92093, United States

V. L. Carvalho-Santos*

*Universidade Federal de Viçosa, Departamento de Física,
Avenida Peter Henry Rolfs s/n, 36570-000, Viçosa, MG, Brasil
(Dated: March 14, 2022)*

Magnetic nanorings have been widely studied due to their potential applications in spintronic and magnonic devices. In this work, by means of analytical calculations and micromagnetic simulations we have analyzed the magnetic energy of nanorings with variable anisotropy along their radius. Four magnetic states, including two new magnetic configurations, here called meron and knot-like states, are considered, looking to the relative lower energy states as a function of anisotropy. Phase diagrams with this states are presented.

I. INTRODUCTION

Due to important applications based on the promising concepts of spintronic and magnonic, nanomagnetism has become an area of intense research in the last decades. In fact, the production of magnetic nanostructures with different shapes and sizes have been reported in several works [1–4]. In this context, magnetic nanorings have become the focus of strong research because of their magnetic behavior. Several works have addressed the static and dynamic properties of ring's magnetization from the theoretical [5–13] as well as from the experimental [14–17] points of view, .

Ring-shaped particles are defined by their external and internal radii, R and r , respectively, and their thickness, h . From magnetic measurements and micromagnetic simulations, three ideal internal magnetic configurations have been identified in such nanostructures: i) the out-of-plane ferromagnetic state (SD_z); ii) the onion (O); and iii) the vortex (V) configurations [6–8, 18–21]. In the SD_z state, the magnetic moments are parallel to the ring axis, whereas in the other two, the magnetization vector field lays parallel to the ring base. The onion state is accessible from an in-plane saturation of the magnetization and it is characterized by the presence of two opposite walls [22]. In the O and SD_z states the ring magnetization is nonzero and then the resulting demagnetizing field leads to deviations in the direction of the magnetic moments close to the particle borders, giving rise to edge domains [23]. In the V state, the magnetic moments circulate around the ring axis, and then most of the magnetic flux is confined within the particle. The absence of the highly energetic core region in rings stabilizes the vortex state [7], leading to simpler and reproducible switching processes. Consequently, the determination of the conditions for occurring the vortex state in nanorings has been regarded as a key point for the production of new magnetic devices[24–26].

The resulting magnetization ground-state in nanomagnets is the result of a competition between dipolar, anisotropy and exchange interactions. The phase diagram describing

anisotropic nanorings [8] reveals that magnetization ground-state depends on the relation R/r and the thickness h of the particle. In fact, an increase in the thickness of the nanoring can lead to the formation of a SD_z state while the increasing in R can favor the formation of O or V states, depending on r . Nevertheless, the presence of an uniaxial anisotropy pointing along the ring axis can reduce the thickness for which the SD_z state becomes the ground-state [27]. Therefore, anisotropy could play a very important role in the determination of the magnetization state in a nanoring.

Recently, a large effort has been made to create novel materials with variable magnetic anisotropy, in which the anisotropy could be controlled by electric field [28–30], temperature [31–33], and ion implantation [34–36]. Moreover, it has been shown that reversal magnetization, and domain-wall movement can be controlled by a defined perpendicular anisotropy gradient in Co/Au multilayers using He⁺ ion-bombardment through a wedged Au stopped layer [37]. Therefore, a magnetic anisotropy gradient has the potential to lead different domain walls and magnetic states. However, a detailed study of the effect of an anisotropy gradient on magnetic nanorings has not been presented yet.

Following these ideas, the focus of this study are ring-shaped nanoparticles with variable anisotropy along their radii. Using analytical calculations and micromagnetic simulations we observe the relative lower energy states of the magnetization, evidencing two new possible magnetic configurations, here called meron and knot states.

This work is organized as follows: in Section II we present the theoretical model used in this work. Section III brings the obtained analytical results and micromagnetic simulations are presented. Finally, in section IV we present the conclusions.

II. THEORETICAL MODEL

Aiming to determine the magnetization ground state of nanorings with variable anisotropy, we will use a continuous theory in which the magnetization is described as a vector

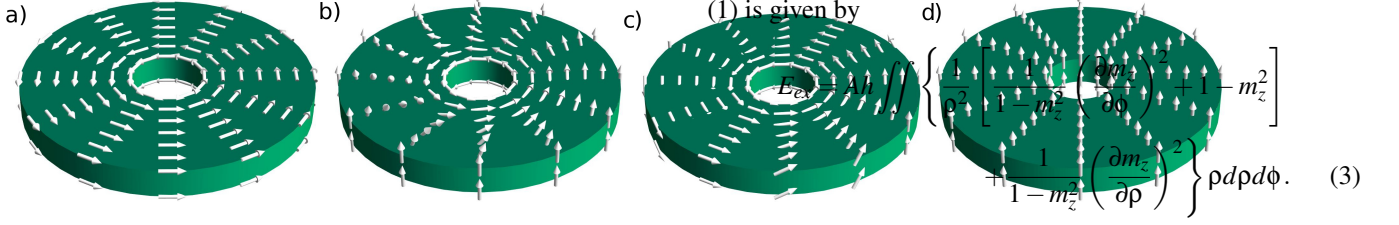


FIG. 1. Magnetic textures a) a vortex, in which all magnetic moments form a close structure. b) a meron-like state, consisting of a vortex state with the magnetic moments gradually pointing upward such that at the external border of the ring $m_z = 1$. c) a state with $\kappa = 1$, consisting in a smooth transition of the magnetic moments going from -1 at the left of the ring to +1 at its right. d) a SD_z configuration. In all figures, $R_{\perp} = R$

field $\mathbf{M}(\mathbf{r})$ consisting of a smooth function of the position \mathbf{r} inside the magnetic body. For our purposes, the magnetization density will be then written as

$$\mathbf{M}(\mathbf{r}) \equiv \mathbf{M} = M_z(\rho, \phi) \hat{z} + M_{\phi}(\rho, \phi) \hat{\phi}, \quad (1)$$

where \hat{z} and $\hat{\phi}$ are unitary vectors in cylindrical coordinates, and $M_z^2 + M_{\phi}^2 = M_S^2$, with M_S the saturation magnetization.

We will consider that the dimensions of the nanoring are such that, for vanishing anisotropy, a vortex configuration is the lower energy state[8]. For non-vanishing anisotropy, four magnetic configurations are studied. Three of them can be described as $m_z = [1 - (R_{\perp} - \rho)^2/R_{\perp}^2]^4 \cos \kappa \phi$ and $m_{\phi} = \sqrt{1 - m_z^2}$, with R and r the external and internal radii of the cylindrical nanoring, respectively. $R_{\perp} \geq R$ is the limit in which the magnetization points parallel to the z -axis in such a way that the larger R_{\perp} the lower the magnetization component along the z -axis direction in the external border of the ring. The value of R_{\perp} will be determined from energy minimization. The three states that can be described by this parametrization are: i) a vortex state (V), obtained in the limit $R_{\perp} \gg R$; ii) a meron-like state (\mathcal{M}), described as a half-skyrmion configuration [40], given by $\kappa = 0$; and iii) a knot-like state (\mathcal{K}) obtained when $\kappa \neq 0$ with the magnetic moments turning around the z -axis when the azimuthal angle is mapped. In this case, κ describes how many times the magnetization vector field rotates around the ring axis direction (z -axis) in the knot state (See Fig. 1). The fourth magnetization texture considered is a single domain state (SD_z) in which the magnetic moments point along the z -axis.

In a continuous approach, the energy (E_{tot}) of a magnetic structure is given by

$$E_{\text{tot}} = A \int (\nabla \mathbf{m})^2 dV - \int K(\rho) m_z^2 dV + \frac{\mu_0 M_S}{2} \int \mathbf{m} \cdot \nabla U(\mathbf{r}) d\mathcal{V}$$

The first, second and third terms in the previous equation correspond to the exchange, dipolar and anisotropy contributions to the magnetic energy, respectively. Here, A is the exchange stiffness, $\mathbf{m} = \mathbf{M}/M_S$, M_S is the saturation magnetization and $K(\rho)$ consists in a radius-dependent anisotropy constant. The exchange energy of the magnetization field described by Eq.

It can be notice that if m_z does not depend on ϕ , Eq. (3) is reduced to

$$E_{ex} = 2\pi Ah \int \left[\frac{1}{1-m_z^2} \left(\frac{\partial m_z}{\partial \rho} \right)^2 + \frac{1-m_z^2}{\rho^2} \right] \rho d\rho \quad (4)$$

according to results presented by Landeros *et al.* [41].

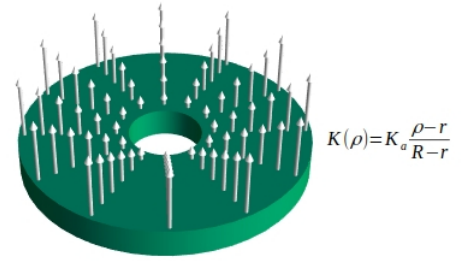


FIG. 2. Profile of the radius-dependent anisotropy. K_a represents the anisotropy value at the ring external border

To determine the dipolar energy of the ring, we need to calculate the magnetostatic potential $U(\mathbf{r})$, which can be determined from the surface and volumetric magnetic charges associated with the magnetization. The surface and volumetric magnetic charges are formally defined as $\sigma = \mathbf{m} \cdot \mathbf{n} = m_z$ and $\mathbf{v} = \nabla \cdot \mathbf{m} = m_z (1 - m_z^2)^{-1/2} \partial_{\phi} m_z$, respectively. In the absence of currents, the magnetostatic potential can be obtained from solving the Laplace equation, whose formal solution is given by $U(\vec{r}) = U_{\sigma} + U_{\mathbf{v}}$, where

$$U_{\sigma} = \frac{M_S}{4\pi} \left\{ \int_{S_1} \frac{\sigma}{|\vec{r} - \vec{r}_1|} dS_1 - \int_{S_2} \frac{m_z}{|\vec{r} - \vec{r}_2|} dS_2 \right\} \quad (5)$$

and

$$U_{\mathbf{v}} = -\frac{M_S}{4\pi} \int \frac{\mathbf{v}}{|\vec{r} - \vec{r}'|} dV, \quad (6)$$

are the magnetostatic potential due to the surface and volumetric magnetostatic charges, respectively. In Eq. (5) S_1 and S_2 are the surfaces of the top and bottom basis of the cylindrical ring and we have assumed that the ring thickness is very small, in such a way that m_z is constant along the z -axis.

In this work we adopt a model in which the magnetic nanoring has an easy-axis anisotropy gradient pointing along the \hat{z} -axis direction and varies linearly with ρ . Thus, the anisotropy term varies in the form $K(\rho) = K_a(\rho - r)/(R - r)$, where K_a is the anisotropy at the external border of the ring (see Fig. 2).

III. RESULTS AND DISCUSSIONS

From the described model, we can calculate the magnetic energy of each magnetization configuration under consideration. The most simple case is the vortex state, since it has vanishing dipolar and anisotropy energies. Then the magnetic energy of a V state can be evaluated only from the exchange contribution

$$E_{\text{exv}} = 2\pi Ah \ln\left(\frac{R}{r}\right). \quad (7)$$

On the other hand, SD_z , \mathcal{M} and \mathcal{K} configurations present magnetostatic charges because they have magnetic moments pointing along the z -axis and, consequently, these states present surface magnetic charges. In this context dipolar and anisotropy energies must be taken into account to determine the magnetic energy of such states. Configurations given by $\kappa \geq 2$ must demand high exchange energy and then, they will not be considered in this work. Thus, aiming to find the phase space of the SD_z , \mathcal{M} and \mathcal{K} states in magnetic nanorings, we will calculate explicitly only the energy associated with $\kappa = 0$ and $\kappa = 1$. We will start calculating the exchange energy of such states. Since the magnetization in this case is ϕ independent, the exchange energy of the \mathcal{M} configuration is obtained from Eq. (4), being evaluated as

$$E_{\text{ex}\mathcal{M}} = 2\pi Ah \int_r^R \left[64 \frac{m_z^{3/2}}{1-m_z^2} \frac{(R_\perp - \rho)^2}{R_\perp^4} - \frac{m_z^2}{\rho^2} \right] \rho d\rho + E_{\text{ex}}(\phi)$$

The \mathcal{K} state given by $\kappa = 1$ represents a state in which the magnetic moments turn once along the z -axis direction when going through the nanoring around the azimuthal angle. Due to the azimuthal dependence of the magnetization configuration, the energy of this state must be calculated from Eq. (3), giving

$$E_{\text{ex}\mathcal{K}} = 2\pi Ah \int \left\{ \left[64 \frac{m_z^{-1/2}}{\sqrt{1-m_z^2}} \frac{(R_\perp - \rho)^2}{R_\perp^4} \right] \times \left(1 - \sqrt{1-m_z^2} \right) - \frac{m_z^2}{2\rho^2} - \frac{\sqrt{1-m_z^2}}{\rho^2} \right\} \rho d\rho + 2E_{\text{exv}}. \quad (9)$$

Now, aiming to determine the magnetostatic energy, we can use the Green's function in cylindrical coordinates to describe the inverse of the distance [39]. After some algebraic manipulation, we can write the magnetostatic potential associated to surface magnetic charges for a generic κ as

$$U_\sigma = \frac{M_s \epsilon_\kappa}{4\pi} \int_r^R \rho' d\rho' m_z(\rho', \phi') \int_0^\infty dq J_\kappa(q\rho) J_\kappa(q\rho') e^{i\kappa\phi} [e^{-q(h-z)} - e^{-q(h+z)}]$$

where $\epsilon_{\kappa=0} = 2\pi$, $\epsilon_{\kappa \neq 0} = \pi$ and $J_\kappa(x)$ is the cylindrical Bessel function of order κ . The substitution of the previous expression into the dipolar term of Eq. (2) yields the magnetostatic energy associated to the surface magnetostatic charge, given by

$$E_\sigma = \frac{\mu_0 M_s^2 \epsilon_\kappa^2}{4\pi} \int_0^\infty dq \left[\int_r^R m_z J_\kappa(q\rho) \rho d\rho \right]^2 (1 - e^{-hq}). \quad (11)$$

It can be noticed that if we consider the \mathcal{M} ($\kappa = 0$) configuration, the above equation is reduced to the magnetostatic energy of the end-width of a skyrmion [40].

The calculation of dipolar energy associated to volumetric magnetostatic charges appearing in the \mathcal{K} state can be performed from the evaluation of the magnetostatic potential given in Eq. (6) for a generic value of κ . In this case, the magnetostatic volumetric charge is evaluated as

$$\mathbf{v} = \nabla' \cdot \mathbf{m}' = \frac{m_z^2 \kappa \cos \kappa \phi' \sin \kappa \phi'}{\sqrt{1 - m_z^2 \cos^2 \kappa \phi'}}. \quad (12)$$

Following the same procedure used to calculate the magnetostatic potential of the surface term, we can expand the inverse of the distance in cylindrical coordinates. Therefore, the volumetric contribution to the magnetostatic potential is given by

$$U_v = \frac{M_s}{4\pi} \int_0^\infty dq \int_0^H dz' e^{-q(z > -z <)} \int_r^R \rho' d\rho' \times \sum_{m=-\infty}^\infty J_m(q\rho') J_m(q\rho) \int_0^{2\pi} \mathbf{v} e^{im(\phi - \phi')} d\phi'. \quad (13)$$

In order to simplify our analysis, we use the property $\cos^2 \kappa \phi' = (1 + \cos 2\kappa \phi')/2$. Thus, we can calculate the integral in ϕ' by using the following series expansion [39]

$$\frac{1}{\sqrt{1 - m_z^2 \cos^2 \kappa \phi'}} = \frac{\sqrt{2}}{m_z} \frac{1}{\sqrt{\cosh \eta - \cos 2\kappa \phi'}} \\ = \frac{2}{\pi m_z} \sum_{n=0}^\infty Q_{n-1/2}^0(\cosh \eta) \cos 2n\kappa \phi', \quad (14)$$

where $\cosh \eta \equiv (2 - m_z^2)/m_z^2$ and $Q_{n-1/2}^0(\cosh \eta)$ is the Legendre function of half-integer order of second kind. In this case, volumetric magnetic charge can be rewritten as

$$\mathbf{v} = \frac{2\kappa m_z}{\pi} \sum_{n=0}^\infty Q_{n-1/2}^0(\cosh \eta) \cos \kappa \phi' \sin \kappa \phi' \cos 2n\kappa \phi'. \quad (15)$$

Substituting the previous expression in Eq. (13), and assuming that κ is an integer and using the properties of integrals of trigonometric functions, we obtain $U_v = 0$. Therefore, the dipolar energy of \mathcal{M} and \mathcal{K} states can be calculated from Eq. (11). The magnetostatic energy of SD_z state has been obtained in Ref. [8].

Finally we determine the anisotropy energy for the \mathcal{M} , \mathcal{K} and SD_z configurations and arbitrary κ values from the third term in Eq. (2)

$$E_{\text{Ani}} = -\epsilon_\kappa h K_a \int_r^R \frac{\rho - r}{R - r} m_z^2 \rho d\rho. \quad (16)$$

Since in the considered parametrization κ is an integer (0 or 1), one can notice that the anisotropy energy of the \mathcal{K} state does not depend on this parameter. Despite the integral in Eq. (16) has analytical solution, it is cumbersome and will be omitted here.

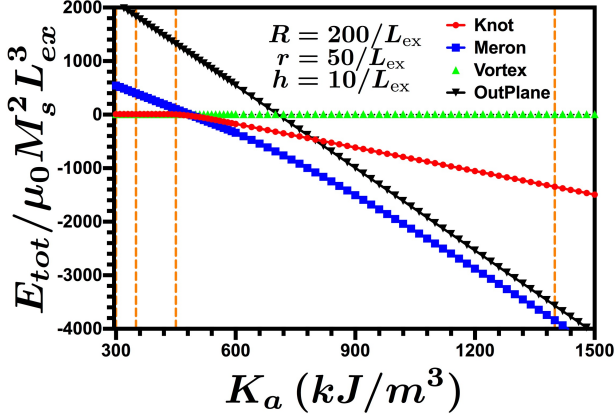


FIG. 3. Magnetic energy of different magnetic states for Permalloy rings as a function of the anisotropy parameter K_a . Results are obtained using $h = 20$ nm, $R = 200$ nm and $r = 50$ nm. Orange dashed lines represents anisotropy values used to perform micromagnetic simulations.

The anisotropy contribution for the SD_z state has a simple analytical expression and can be evaluated as

$$E_{\text{Ani}} = -\frac{\pi h K_a}{3} (R - r)(2R + r). \quad (17)$$

Aiming to perform a subtle analysis of Eqs. (8), (9) and (11) we have solved the integrals numerically. The nominal magnetic parameters associated to Permalloy are used; that is, $A = 1.3 \times 10^{-11}$ J/m, $M_S = 8.6 \times 10^5$ A/m, $\mu_0 = 4\pi \times 10^{-7}$ J/mA² and exchange length $\ell_{\text{ex}} = 5.3$ nm. Such values enables to stabilize all considered magnetization configurations by changing K_a values. Our results for the energies, considering the different configurations are illustrated in Fig. 3. These results evidence that, despite the curves for V and \mathcal{K} states are practically superimposed for $K_a < 450$ kJ/m³, there is a small difference in the energies of these magnetic states. In fact, the V state minimizes the energy for $K_a < 350$ kJ/m³ but when the anisotropy increases, \mathcal{K} state is the configuration the minimizes the total energy. Despite the \mathcal{K} state presents lower magnetostatic energy when compared to the \mathcal{M} state, the difference of the anisotropy energy can stabilize the \mathcal{M} configuration for $k_a > 700$ kJ/m³. It can be observed that this magnetization pattern is highly stable compared to the SD_z configuration in such a way that SD_z state does not minimize the total energy in the range of evaluated K_a values.

To corroborate our analytical results, we have performed micromagnetic simulations using the 3D Object Oriented MicroMagnetic Framework (OOMMF) package [42], which solves the Landau-Lifshitz-Gilbert [43, 44] equation using finite element methods.

Simulations were run using a mesh size of $2 \times 2 \times 2$ nm³ and a damping constant of 0.5. Aiming to allow the system to

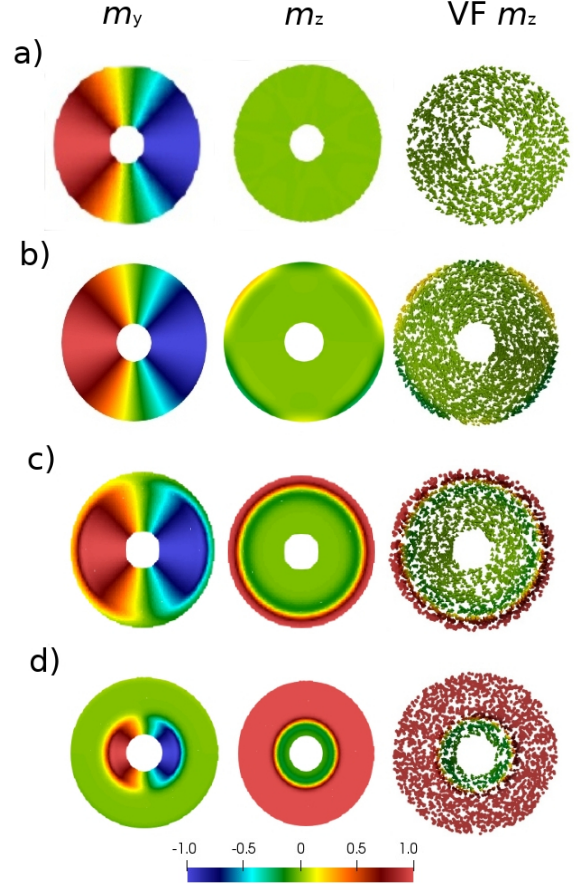


FIG. 4. Final states for different anisotropies from OOMMF simulations. From left to right we show the magnetization components m_y , m_z and the vector field (VF). Results obtained for a) $K_a = 300$ kJ/m³, b) $K_a = 350$ kJ/m³, c) $K_a = 450$ kJ/m³ and d) $K_a = 1400$ kJ/m³.

reach equilibrium, we have used a usual torque condition that establishes when simulations can stop. That is, the minimum energy state is reached when the torque on the magnetic moments is below 0.001 A/m. Our simulations were performed starting from four different initial configurations: i) a V configuration; ii) a state in which half of the ring is in a vortex state and the other half with two opposite saturated configurations; iii) a state in which the magnetization in half of the ring is a vortex state and in the other half magnetic moments are pointing along the z -axis; and iv) a single domain pointing along the xy -plane. The energy of the final state associated with each initial configuration was calculated, leading us to obtain the lower energy state for each K_a value.

We have then simulated magnetic nanorings with four different anisotropy parameters: 300 kJ/m³, 350 kJ/m³, 450 kJ/m³ and 1400 kJ/m³. The final states are shown in Fig. 4. It can be noticed that the magnetic configuration of the lower energy states agrees with the magnetic configuration of the lower energy state from analytical calculations. Nevertheless, it can be observed that the final \mathcal{K} state (Fig. 4-b) is differ-

ent from that one described in the analytical model. Indeed, while our analytical model predicts a \mathcal{K} state in which the region with out-of-plane components of the magnetization has the same area that the region with in-plane components, the analysis of Fig. 4b shows that the area occupied by the out-of-plane component of the \mathcal{K} state is larger than the in-plane one. However, the mathematical formalism describing such configuration leads to cumbersome equations and does not present different qualitative changes with the obtained phase diagram. Another important observation coming from the analysis of Fig. 4c and 4d is that the region of the out-of-plane component to the magnetization for \mathcal{M} state increases with the anisotropy in such a way that for very high values of K_a , a SD_z state can be observed. That is, by increasing the anisotropy the region of the out-of-plane component of the magnetization occupy a larger area of the ring. This finding reveals that the region occupied by the out-of-plane component can be controlled by varying the anisotropy at the border of the ring.

IV. CONCLUSIONS

In this work we have studied the possible magnetic ground-state of a nanoring having an anisotropy gradient along its ra-

dius. We have analytically calculated the magnetic energy of four different magnetization configurations and have obtained the energy curves in function of the anisotropy for each considered magnetization configuration. We have also performed micromagnetic simulations and analyzed the possibility of obtaining two new magnetic configurations in magnetic nanorings, the so called meron and knot-like states.

The possibility of obtaining the \mathcal{M} and \mathcal{K} states in nanomagnetic systems is very interesting, from the fundamental and the applied points of view. From the fundamental point of view, is always an important issue the appearance of new magnetic textures. From the applied perspectives, the existence of different magnetic configurations may be associated with new properties that could allow applications in technological developments based on the concept of spintronic and magnonic. Due to emergent new experimental techniques controlling magnetic anisotropy gradient, such new states could be observed.

We thank Brazilian agency CNPq for financial support (grant numbers 401132/2016-1 and 301015/2015-5). In Chile we acknowledge Fondecyt under grants 1160198, and the Basal program under grant FB 0807. N. M. Vargas acknowledges the financial support from the Department of Energy's Office of Basic Energy Science under grant DE-FG02-87ER-45332.

* vagson.carvalho@usach.cl

- ¹ R.P. Cowburn, J. Phys. **D 33**, R1 (2000).
- ² R. Streubel, V.P. Kravchuk, D.D. Sheka, D. Makarov, F. Kronast, O.G. Schmidt, and Y. Gaididei, Appl. Phys. Lett. **101**, 132419 (2012).
- ³ R. Streubel, D.J. Thurmer, D. Makarov, F. Kronast, T. Kosub, V.P. Kravchuk, D.D. Sheka, Y. Gaididei, R. Schäfer, and O.G. Schmidt, Nano Lett. **12**, 3961 (2012).
- ⁴ I. Minguez-Bacho, S. Rodríguez-López, M. Vázquez, M. Hernández-Vélez, and K. Nielsch, Nanotechnology **25**, 145301 (2014).
- ⁵ P. Landeros, S. Allende, J. Escrig, E. Salcedo, D. Altbir, and E. E. Vogel, Appl. Phys. Lett. **90**, 102501 (2007).
- ⁶ M. Beleggia, J.W. Lau, M.A. Schofield, Y. Zhu, S. Tandon, and M. De Graef, J. Magn. Mag. Mat. **301**, 131 (2006).
- ⁷ V.P. Kravchuk, D.D. Sheka, and Y.B. Gaididei, J. Magn. Mag. Mat. **310**, 116 (2007).
- ⁸ P. Landeros, J. Escrig, D. Altbir, M. Bahiana, and J. d'Albuquerque e Castro, J. Appl. Phys. **100**, 044311 (2006).
- ⁹ V.L. Carvalho-Santos, W.A. Moura-Melo, and A. R. Pereira, J. Appl. Phys. **108**, 094310 (2010).
- ¹⁰ S. Castillo-Sepúlveda, N.M. Vargas, R. Escobar, S. Allende, S. Baltazar, and D. Altbir, J. Appl. Phys. **115**, 223903 (2014).
- ¹¹ A. Riveros, N. Vidal-Silva, P. Landeros, D. Altbir, E.E. Vogel, J. Escrig J. Mag. Mag. Mat. **401**, 848 (2016).
- ¹² S. Vojkovic, A.S. Nunez, D. Altbir, and V.L. Carvalho-Santos, J. Appl. Phys. **120**, 033901 (2016).
- ¹³ S. Vojkovic, V.L. Carvalho-Santos, J.M. Fonseca, and A.S. Nunez, J. Appl. Phys. **121**, 113906 (2017).
- ¹⁴ J. Rothman, M. Kläui, L. Lopez-Diaz, C.A.F. Vaz, A. Bleloch, J.A.C. Bland, Z. Cui, and R. Speaks, Phys. Rev. Lett. **86**, 1098 (2001).
- ¹⁵ M. Kläui, C.A.F. Vaz, L. Lopez-Diaz, and J.A. C. Bland, J. Phys.: Condens. Matter **15**, R985 (2003).
- ¹⁶ F. Q. Zhu, G. W. Chern, O. Tchernyshyov, X. C. Zhu, J. G. Zhu, and C. L. Chien Phys. Rev. Lett. **96**, 027205 (2006).
- ¹⁷ C.A.F. Vaz, T.J. Hayward, J. Llandro, F. Schackert, D. Morecroft, J.A.C. Bland, M. Kläui, M. Laufenberg, D. Backes, U. Rüdiger, F.J. Castaño, C.A. Ross, L.J. Heyderman, F. Nolting, A. Locatelli, G. Faini, S. Cherifi, and W. Wensdorfer, J. Phys.: Condens. Matter **19**, 255207 (2007).
- ¹⁸ M. Grimsditch, Y. Jaccard, and I. K. Schuller, Phys. Rev. B **58**, 11539 (1998).
- ¹⁹ M. C. Abraham, H. Schmidt, T. A. Savas, H. I. Smith, C. A. Ross, and R. J. Ram, J. Appl. Phys. **89**, 5667 (2001).
- ²⁰ M. Hwang, M. C. Abraham, T. Savas, H. I. Smith, R. J. Ram, and C. A. Ross, J. Appl. Phys. **87**, 5108 (2000).
- ²¹ R. P. Cowburn, D. K. Koltsov, A. O. Adeyeye, M. E. Welland, and D. M. Tricker, Phys. Rev. Lett. **83**, 1042 (1999).
- ²² F. J. Castaño, C.A. Ross, C. Frandsen, A. Eilez, D. Gil, H. I. Smith, M. Redjbal, and F. B. Humphrey, Phys. Rev. **B 67**, 184425 (2003).
- ²³ A. Lebib, S.P. Li, M. Natali, and Y. Chen, J. Appl. Phys. **89**, 3892 (2001).
- ²⁴ L. Xiao-Li, Y. Yong, W. Jian-Peng, Z. Yi-Fan, F. Hai-Ming, and D. Jun, Chinese Phys. **B 24**, 127505 (2015).
- ²⁵ X.L. Liu, Y. Yang, C.T. Ng, L.Y. Zhao, Y. Zhang, B.H. Bay, H.M. Fan, J. Ding, Adv. **27**, 1939 (2015).
- ²⁶ C.S.B. Dias, T.D.M. Hanchuk, H. Wender, W.T. Shigeyosi, J. Kobarg, A.L. Rossi, M.N. Tanaka, M.B. Cardoso, and F. Garcia, Sci. Rep. **7**, 14847 (2017).
- ²⁷ W. Zhang, R. Singh, N. Bray-Ali, and S. Haas, Phys. Rev. **B 77**, 144428 (2008).
- ²⁸ S. Miwa, K. Matsuda, K. Tanaka, Y. Kotani, M. Goto, T. Nakamura, and Y. Suzuki, Appl. Phys. Lett. **107**, 162402 (2015).
- ²⁹ T. Nozaki, A. Koziol-Rachwal, W. Skowroński, V. Zayets, Y.

- Shiota, S. Tamaru, H. Kubota, A. Fukushima, S. Yuasa, and Y. Suzuki, *Phys. Rev. Appl.* **5**, 044006 (2016).
- ³⁰ M. Weisheit, S. Fähler, A. Marty, Y. Souche, C. Poinsignon, and D. Givord, *Science* **315**, 349 (2007).
- ³¹ J.G. Ramírez, J. de la Venta, S. Wang, T. Saerbeck, A.C. Basaran, X. Batlle, and I.K. Schuller, *Phys. Rev.* **B 93**, 214113 (2016).
- ³² J. de la Venta, S. Wang, T. Saerbeck, J.G. Ramírez, I. Valmianski, and I.K. Schuller, *Appl. Phys. Lett.* **104**, 062410 (2014).
- ³³ D.A. Gilbert, J.G. Ramírez, T. Saerbeck, J. Trastoy, I.K. Schuller, K. Liu, and J. de la Venta, *Sci. Rep.* **7**, 13471 (2017).
- ³⁴ T. Amarouche, L.-C. Garnier, M. Marangolo, M. Eddrief, V.H. Etgens, F. Fortuna, Y. Sadaoui, M. Tamine, J.L. Cantin, and H.J. von Bardeleben, *J. Appl. Phys.* **121**, 243903 (2017).
- ³⁵ M. Jaafar, R. Sanz, J. McCord, J. Jensen, R. Schafer, M. Vazquez, and A. Asenjo, *Phys. Rev.* **B 83**, 094422 (2011).
- ³⁶ Y. Yuan, T. Amarouche, C. Xu, A. Rushforth, R. Böttger, K. Edmonds, R. Campion, B. Gallagher, M. Helm, H.J. von Bardeleben, *J. Phys. D: Appl. Phys.* **51**, 145001 (2018).
- ³⁷ M. Urbaniak, P. Kuświk, Z. Kurant, M. Tekielak, D. Engel, D. Lengemann, B. Szymański, M. Schmidt, J. Aleksiejew, A. Maziewski, A. Ehresmann, and F. Stobiecki *Phys. Rev. Lett.* **105**, 067202 (2010)
- ³⁸ G. Goia, and R.D. James, *Proc. R. Soc. A* **453**, 213 (1997); R. Kohn, and V. Slastikov, *Proc. R. Soc. A* **461**, 143 (2005).
- ³⁹ P. Morse, and H. Feshbach, “Methods of Theoretical Physics”, Mc. Graw-Hill, 1st ed., New York, (1953).
- ⁴⁰ M.A. Castro, and S. Allende, *J. Magn. Mag. Mat.* **417**, 344 (2016).
- ⁴¹ P. Landeros, J. Escrig, D. Altbir, D. Laroze, J. d’Albuquerque e Castro, and P. Vargas, *Phys. Rev.* **B 71**, 094435 (2005).
- ⁴² M.J. Donahue, and D.G. Porter, National Institute of Standards and Technology Interagency Reports NISTIR 6376 (1999).
- ⁴³ L. Landau, and E. Lifshitz, *Ukr. J. Phys.* **53**, 14 (2008). Reprinted from *Phys. Zeitsch. der Sow.* **8**, 153 (1935).
- ⁴⁴ T.L. Gilbert, *IEEE Trans. on Magnetism* **40**, 3443 (2004).